

Retrieving missing data in electron diffraction of gas-phase molecules

Yanwei Xiong*, Nikhil Kumar Pachisia, Martin Centurion†

Department of Physics and Astronomy, University of Nebraska-Lincoln, Lincoln, Nebraska, 68588, USA

ABSTRACT. We report an iterative algorithm to retrieve accurate real space information from gas electron diffraction measurements with missing data at low momentum transfer. The algorithm is similar to phase retrieval algorithms which transform signals back and forth between the signal domain and the Fourier domain and apply constraints to retrieve the missing phase. The difference in our case is that the goal is not retrieval of the phase of the diffraction signal but the missing data at low momentum transfer, which is necessary for generating the real-space pair distribution function. The missing data is a common problem in static and ultrafast gas phase electron diffraction experiments due to experimental constraints. We demonstrated successful restoration of the missing data in simulated data and in experimentally measured diffraction signals of static and photo-dissociated trifluoroiodomethane and iodobenzene molecules.

I. INTRODUCTION.

Gas phase ultrafast electron diffraction (GUED) has demonstrated the capability to determine the structures of isolated molecules and to capture their nuclear motions during chemical reactions with femtosecond and sub-angstrom resolutions [1, 2]. In GUED experiments, a pump laser is used to excite the molecules and initiate a chemical reaction, and a probe, either an electron pulse with a kinetic energy of keV [3-7] or MeV [8-11], is used to interrogate the evolving structure of the photoexcited molecules. The time delay between the laser pulse and electron pulse is adjusted by an optical delay line to take a series of diffraction patterns, from which the evolving structure can be extracted [12].

The analysis of GUED can be relegated to one-dimensional (1-D) signals in both the momentum transfer and real space domains, allowing for retrieval of changes in the interatomic distances of the reacting molecules. In this 1-D analysis, the Fourier sine transform of the modified diffraction intensity (sM) produces the pair distribution function (PDF), which gives the interatomic distances, or their changes, in real space [5, 13-15]. Two-dimensional (2-D) diffraction signals captured by GUED have been used to obtain additional information about molecular reactions, such as the determination of interatomic distances and bond angles of molecules in the ground state [16-18], measurement of atom-pair angular distributions [4, 19, 20], and observation of transient molecular structures formed during laser induced reactions [21-23]. For molecules in an anisotropic angular distribution, the 2D-PDF has been developed to obtain structural information in real space, including interatomic distances and atom-pair angular distributions [4, 17, 20, 22]. The 2D-PDF is produced by the inverse Fourier transform, followed by an Abel inversion, of the 2-D $sM(s)$.

While the technique of GUED data analysis has allowed us to obtain structural information in real space, the retrieval of real space information is limited in part by the inability to measure the GUED experimental diffraction signal at low scattering angles. This is due to the limited size of the electron pulses and the low scattering cross-section of gas phase samples. The small scattering cross-section for high-energy electrons leads to most electrons passing straight through the sample without any interaction. A beam stop is required to block the transmitted electron beam [3, 9, 24-26] to avoid un-scattered electrons bombarding the detector, which causes saturation on the detector while it is used to capture the scattered electrons that produce a much weaker signal. Therefore, the diffraction signal around 0\AA^{-1} which is overlapped with the transmitted electron beam is unavailable. The PDF cannot be produced accurately without the signal at the low scattering angle.

Different methods have been developed to fill in the missing data in the region around 0\AA^{-1} . One option is to fill the missing data by smooth interpolation to zero at the origin [17, 27]. While this method avoids biasing structure retrieval, it could introduce artifacts in the PDF. Another method is to fill the missing region with the theoretically calculated sM [3, 5, 13, 14, 17, 28-31]. This method is useful and easy to apply for unexcited molecules since the structures are known, and static diffraction signal can be calculated. However, for time-resolved structural analysis, this method requires expensive computations for structure search and refinement by comparing the theoretical sM of all possible structures to the experimental sM [5, 13, 14, 28, 29]. In the case of multiple reaction channels present in the chemical reaction, the structure search and refinement become challenging.

In this work, we introduce an iterative algorithm to retrieve the electron diffraction signal in the missing region with the available signal measured by GUED.

The iterative algorithm is adapted from the ideas of existing phase retrieval algorithms, like the Gerchberg-Saxton algorithm, error-reduction algorithm and hybrid input-output algorithm [32-37]. These algorithms iteratively transform data back and forth between the object domain and the Fourier domain through Fourier transform and inversion, applying known constraints in each domain while allowing the phase to be adjusted until a solution is found [32, 38]. These ideas have also been used to reconstruct X-ray crystallography images solely from diffraction patterns [37, 39].

Here we test the retrieval algorithm by restoring the 1-D diffraction data produced by a random distribution of isolated molecules as a sample. The sM consists of a series of sinusoidal functions modulated by the scattering amplitudes of the corresponding atoms. The available sM signal contains information about the interatomic distances of the molecule. However, due to the missing data at low scattering angles, the PDF, which is the Fourier sine transform of the sM , contains artifacts. The artifacts that correspond to the Fourier domain usually have a broad distribution since the missing region of the data is small. The artifacts can be reduced by applying constraints to the PDF using prior knowledge of the molecule, such as knowing the range of possible interatomic distances present in the molecular structure. We iteratively transform the signal back and forth between the sM and the PDF through Fourier sine transform, enforcing known constraints to reduce the artifacts in each iteration while allowing the signal to converge until the artifacts cannot be further reduced. In doing so, the sM of the missing region at low scattering angles can be restored. We first tested the retrieval algorithm with the simulated signals of trifluoriodomethane and iodobenzene. We then applied the algorithm to successfully retrieve the missing data in the experimental diffraction signals of static and photo-dissociated trifluoriodomethane and iodobenzene molecules. Note that the method described here can in principle also be used to retrieve the low scattering angle data in gas phase X-ray scattering signals.

II. THEORY

In this section, we first review the electron scattering theory for gas phase molecules. We then describe the iterative algorithm that restores the unavailable low momentum transfer data in electron scattering measurements using the available diffraction signal.

A. Electron scattering theory

The conventional theory of electron scattering from isolated molecules has been described in detail

previously [5, 40-43]. The elastic diffraction from a neutral molecule can be well approximated using the independent atom model (IAM), in which the bonding effects are neglected and the potential of each atom that constitutes the molecule is assumed to be spherically symmetric [40, 44, 45]. In electron scattering from isolated molecules, electron waves scattered from the atoms within the same molecule interfere. The elastic scattering intensity of a single molecule that consists of N atoms is given by

$$I(\mathbf{s}) = \sum_{j=1}^N \sum_{k=1}^N f_j^*(\mathbf{s}) f_k(\mathbf{s}) e^{i\mathbf{s} \cdot \mathbf{r}_{jk}}, \quad (1)$$

where $f_j(\mathbf{s})$ is the atomic scattering amplitude of the j^{th} atom [46, 47], \mathbf{r}_{jk} is a vector pointing from the k^{th} atom to the j^{th} atom with length equal to the interatomic distance, and \mathbf{s} is the momentum transfer vector of the scattered electron. The total elastic diffraction intensity from a gas phase sample, which contains a larger number of molecules, is an incoherent sum of the scattering signals from all the molecules in the ensemble, given by [4, 12, 20]

$$I_{\text{total}}(\mathbf{s}) = \iint \sum_{j=1}^n \sum_{k=1}^n f_j^*(\mathbf{s}) f_k(\mathbf{s}) e^{-i\mathbf{s} \cdot \mathbf{r}_{jk}(\alpha, \beta)} \times g_{jk}(\alpha, \beta) \sin\alpha \, d\alpha d\beta, \quad (2)$$

where α, β are the polar and azimuthal angles that describe the atom pair jk of a molecule in the lab frame, and $g_{jk}(\alpha, \beta)$ is the angular distribution of atom pair jk . The relation of the atom-pair angular distribution and probability density of the molecular orientation, which is a function of the Euler angles, is given by equation (1) in ref. [12, 20]. The angular distribution can usually be reduced to $g_{jk}(\alpha)$ when it is cylindrically symmetric.

Eqn (2) can be further separated as $I_{\text{total}}(\mathbf{s}) = I_A(\mathbf{s}) + I_M(\mathbf{s})$. The first term is the atomic scattering term given by the sum of the terms with $j = k$ in Eqn (2), formulated as $I_A(\mathbf{s}) = \sum_{j=1}^N |f_j(\mathbf{s})|^2$, which contains no information about the structure of the molecule. The second term is the molecular scattering term $I_M(\mathbf{s})$, given by the sum of terms with $j \neq k$ in Eqn (2), in which the structural information of the molecule and the angular distribution of atom pairs are encoded. For an ensemble of molecules with a random distribution, the atom-pair angular distributions are given by $\frac{1}{4\pi}$. Eqn (2) becomes [48, 49]

$$I_M(\mathbf{s}) = \sum_{j=1}^N \sum_{k \neq j}^N f_j^*(\mathbf{s}) f_k(\mathbf{s}) \frac{\sin(sr_{jk})}{sr_{jk}}. \quad (3)$$

In this case, the two-dimensional (2-D) molecular scattering pattern consists of a series of concentric rings with an amplitude that decreases approximately as s^{-5} as s increases. The 2-D pattern usually is azimuthally averaged to obtain the 1-D molecular

scattering term $I_M(s)$ with a higher fidelity. The modified scattering intensity $sM(s)$ is introduced to remove the rapidly decreasing trend and highlight the oscillations in the signal [13, 43]

$$sM(s) = \frac{sI_M(s)}{I_A(s)}. \quad (4)$$

The interatomic distances r_{jk} can be obtained by applying a Fourier sine transform to the $sM(s)$ to produce the pair distribution function (PDF) [13, 43], given by

$$\text{PDF}(r) = \int_0^{s_{\max}} sM(s) \sin(sr) e^{-ds^2} ds, \quad (5)$$

where s_{\max} is the maximum amplitude of the momentum transfer vector of the scattered electron recorded by the detector. A dampening term, e^{-ds^2} , is included to reduce the artifacts due to the discontinuity of the signal at s_{\max} .

For an ensemble of molecules with atom-pair angular distributions that depend on one angle, both the $g_{jk}(\alpha)$ and intranuclear distances r_{jk} can be obtained by applying a 2-D Fourier transform followed by an Abel inversion to the 2-D modified scattering intensity $sM(s)$ [4, 20, 22]. For randomly distributed molecules, the 2-D signal as a function of s relegates to 1-D signal that depends on the scalar s . In this work, we focus on retrieving the missing data of 1-D diffraction signals.

In GUED measurements, we investigate the changes of the molecular structure by calculating the diffraction difference intensity

$$\Delta I_M(s, t) = I_{\text{total}}(s, t) - I_{\text{total}}(s, t_0), \quad (6)$$

where the variable t denotes the time delay with respect to the laser excitation. $I_{\text{total}}(s, t_0)$ is the total scattering intensity at time t_0 , which corresponds to a time before the arrival of the laser pulse, i.e. before the sample is excited [5, 17]. Correspondingly, the $\Delta sM(s)$ can be defined as

$$\Delta sM(s, t) = s\Delta I_M(s, t)/I_A. \quad (7)$$

B. Retrieval method

In this section, we describe the iterative algorithm to restore the missing data in electron diffraction measurement. First, we describe the sM and PDF as Fourier sine transform pairs by defining an odd function that corresponds to the sM . Second, we mathematically model the practical experimental electron diffraction signal and the artifact term. Third, we demonstrate the technique of using a band-pass filter as a constraint to reduce the artifact term based on prior knowledge of the molecule.

Based on eqn (4) and eqn (5), we define an odd function $\mathcal{M}(s)$ by extending the variable s from $0 \leq s \leq s_{\max}$ to $-s_{\max} \leq s \leq s_{\max}$. The odd function $\mathcal{M}(s)$ is given by

$$\mathcal{M}(s) = \begin{cases} \sum_{j=1}^N \sum_{k \neq j}^N c_{jk}(s) \sin(sr_{jk}) & \text{for } |s| \leq s_{\max} \\ 0 & \text{otherwise} \end{cases} \quad (8)$$

where $c_{jk}(s) = f_j^*(s)f_k(s)/(I_A r_{jk})$. Note that the negative s is only mathematically meaningful. The function $\mathcal{M}(s)e^{-ds^2}$ is an odd function, and the Fourier sine transform, and its inversion are

$$\mathcal{P}(r) = \int_0^{+\infty} \mathcal{M}(s) e^{-ds^2} \sin(sr) ds, \quad (9)$$

$$\mathcal{M}(s) e^{-ds^2} = \frac{2}{\pi} \int_0^{+\infty} \mathcal{P}(r) \sin(sr) dr. \quad (10)$$

The $sM(s)$ given by eqn (4) is identical to the function $\mathcal{M}(s)$ for $s \geq 0$. Therefore $\mathcal{P}(r)$ in eqn (9) is equal to the $\text{PDF}(r)$ given in eqn (5). In practical diffraction experiments, a beam block before the detector [3, 24, 25] or a hole in the detector [9, 26] is used to avoid the un-scattered electrons bombarding the detector. Therefore, the diffraction signal in the low s range around 0 \AA^{-1} is unavailable. Suppose the range of the missing data is from 0 to s_a , and we usually fill the missing region by smooth interpolation to zero at the origin. The signal of this missing part from 0 to s_a is a linear function, given by $s\mathcal{M}_e(s_a)/s_a$, which is different from $\mathcal{M}(s)$ for s from 0 to s_a . Similar to eqn (8), an odd function $\mathcal{M}_e(s)$ that corresponds to the measured diffraction signal with a linear filling at the missing region can be defined as

$$\mathcal{M}_e(s) = \begin{cases} \sum_{j=1}^N \sum_{k \neq j}^N c_{jk}(s) \sin(sr_{jk}) & \text{for } s_a \leq |s| \leq s_{\max} \\ \frac{\mathcal{M}_e(s_a)}{s_a} \times s & \text{for } |s| < s_a \\ 0 & \text{otherwise} \end{cases} \quad (11)$$

Similar to the Fourier sine transform pairs given in eqn (9) and eqn (10), the experimental PDF $\mathcal{P}_e(r)$ is the Fourier sine transform of $\mathcal{M}_e(s)e^{-ds^2}$ and the inverse transform of $\mathcal{P}_e(r)$ gives $\mathcal{M}_e(s)e^{-ds^2}$. The $\mathcal{P}_e(r)$ is given by

$$\mathcal{P}_e(r) = \mathcal{P}(r) + \mathcal{A}(r), \quad (12)$$

where $\mathcal{A}(r)$ is the artifact caused by the signal in the missing region, which is different from the real signal from 0 to s_a , and $\mathcal{A}(r)$ is given by

$$\mathcal{A}(r) = \int_0^{s_a} \left[\frac{s\mathcal{M}_e(s_a)}{s_a} - \mathcal{M}(s) \right] e^{-ds^2} \sin(sr) ds. \quad (13)$$

Also, we have the following relation

$$[\mathcal{M}_e(s) - \mathcal{M}(s)] e^{-ds^2} = \frac{2}{\pi} \int_0^{+\infty} \mathcal{A}(r) \sin(sr) dr. \quad (14)$$

The goal of this work is to reduce $\mathcal{A}(r)$ to a value close to zero through iterations so that we can restore $\mathcal{M}(s)$ and $\mathcal{P}(r)$ using the experimental diffraction signal $\mathcal{M}_e(s)$. Therefore, the data in the missing region can be restored.

The conditions that allow the diffraction signal in the missing region to be restored are listed below. (a) The s -range ($s_a \sim s_{max}$) of the available signal needs to be big enough to approximately resolve the distribution of the interatomic distances r_{jk} . (b) The s -range ($0 \sim s_a$) of missing region should be relatively small so that the distribution of the artifact term $\mathcal{A}(r)$ has a broader distribution than that of $\mathcal{P}(r)$. (c) Some prior knowledge of the molecule is known, so that the minimum and maximum interatomic distances can be approximately determined.

Using the prior knowledge of the molecule, a band-pass filter (constraints) is applied to select the distribution of the interatomic distances r_{jk} in $\mathcal{P}_e(r)$ and remove the part of $\mathcal{A}(r)$ that is not overlapped with the distribution of distances r_{jk} . This operation reduces the artifact term $\mathcal{A}(r)$. A new $\mathcal{M}_e(s)$ can be produced by the Fourier sine inverse transform of the filtered $\mathcal{P}_e(r)$, and the difference between new $\mathcal{M}_e(s < s_a)$ and original $\mathcal{M}(s < s_a)$ is reduced as part of $\mathcal{A}(r)$ is removed. The new $\mathcal{M}_e(s < s_a)$ can be used to fill the missing region ($s < s_a$) of the experimental signal and to generate $\mathcal{P}_e(r)$ again, followed by the filtering operation. In each iteration, the $\mathcal{A}(r)$ term tends to have a broad distribution. Therefore, by iterating these processes many times, the difference between $\mathcal{M}_e(r < s_a)$ and $\mathcal{M}(r < s_a)$ is reduced so that $\mathcal{P}_e(r)$ approaches $\mathcal{P}(r)$.

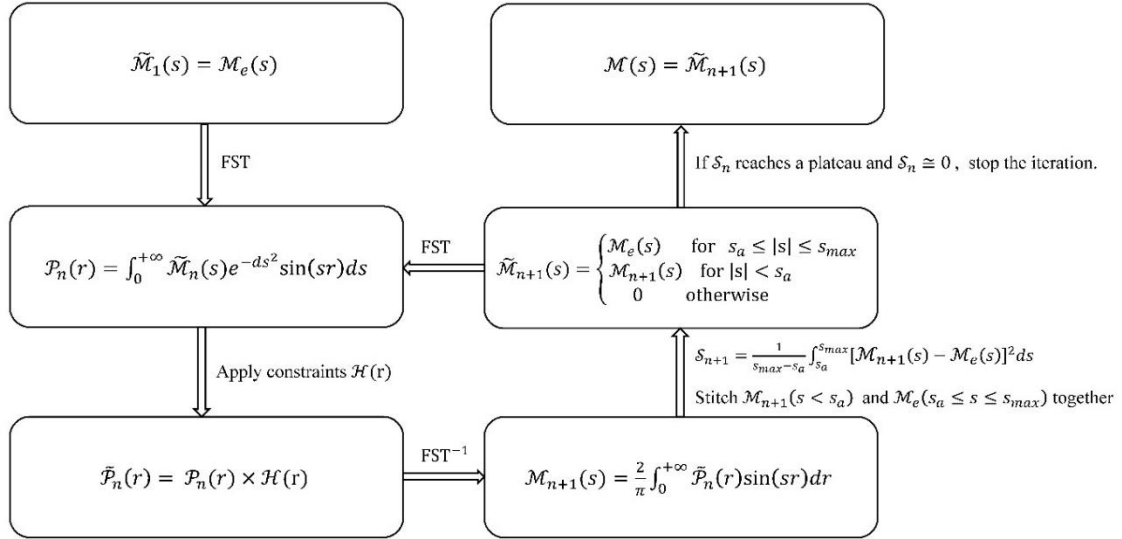


Figure 1. Block diagram showing the retrieval of the data in the missing region through iterations. The iteration number is denoted by n . FST stands for Fourier sine transform, given by Eqn (9). FST⁻¹ stands for the Fourier sine inverse transform, given by Eqn (10).

Figure 1 shows the block diagram of the iterative algorithm that restores the data in the missing region. The steps are listed below. (a) For $n=1$, $\tilde{\mathcal{M}}_1(s) = \mathcal{M}_e(s)$, where $\mathcal{M}_e(s)$ is given by Eqn (11). (b) We apply the Fourier sine transform to $\tilde{\mathcal{M}}_n(s)$ to generate $\mathcal{P}_n(r)$. The artifact term $\mathcal{A}(r)$ has a broader distribution than $\mathcal{P}(r)$. (c) We use a band-pass filter $\mathcal{H}(r)$, which is defined by the rough prior knowledge about the molecule, to reduce the artifact term $\mathcal{A}(r)$ and produce $\tilde{\mathcal{P}}_n(r)$. (d) A Fourier sine inverse transform is applied to $\tilde{\mathcal{P}}_n(r)$ to generate $\mathcal{M}_{n+1}(s)$. (e) We stitch $\mathcal{M}_{n+1}(s < s_a)$ and $\mathcal{M}_e(s_a \leq s \leq s_{max})$ together to produce $\tilde{\mathcal{M}}_{n+1}(s)$, in which the signal in the missing region is improved compared to $\tilde{\mathcal{M}}_n(s)$.

The signal with artifacts is constrained in the s range $0 < s < s_a$. To avoid discontinuity in $\tilde{\mathcal{M}}_{n+1}(s)$, the signal $\mathcal{M}_{n+1}(s < s_a)$ is multiplied by a value given by $\int_{s_a}^{s_a+\varepsilon} \mathcal{M}_e(s) ds / \int_{s_a-\varepsilon}^{s_a} \mathcal{M}_{n+1}(s) ds$, where ε is a small value, such as 0.01 \AA^{-1} . (f) Repeat step (b) by replacing $\tilde{\mathcal{M}}_n(s)$ with $\tilde{\mathcal{M}}_{n+1}(s)$ to generate $\mathcal{P}_{n+1}(r)$ and $\tilde{\mathcal{P}}_{n+1}(r)$, followed by step (c-e). (g) We calculate the sum of square differences in each iteration to determine when to stop the iteration, given by

$$\mathcal{S}_n = \frac{1}{s_{max}-s_a} \int_{s_a}^{s_{max}} [\mathcal{M}_n(s) - \mathcal{M}_e(s)]^2 ds. \quad (15)$$

The $\mathcal{M}_e(s)$ from s_a to s_{max} is the experimental measurement of $\mathcal{M}(s_a < s < s_{max})$. Therefore,

$\mathcal{M}_n(s)$ approaches to $\mathcal{M}_e(s)$ when the artifact term $\mathcal{A}(r)$ is minimized to a value close to zero according to eqn (14). If \mathcal{S}_n reaches a plateau and $\mathcal{S}_n \cong 0$, it means that the artifact term $\mathcal{A}(r)$ cannot be further reduced, and we stop the iteration.

III. TEST WITH SIMULATED SIGNAL

In this section, we test the iterative algorithm described in II.B using a calculated diffraction signal. The kinetic energy of the electrons used in the calculation is 90 keV, and the scattering amplitude of the atoms are tabulated in [50]. We use eqn (3) and (4) to calculate the $sM(s)$ and select the s -range $s_a \leq s \leq s_{max}$ of the data as the available signal. In practical UED experiments, the s -range of useful data is commonly from around 1\AA^{-1} to 10\AA^{-1} [3, 9]. With the $sM(s)$ for $s_a \leq s \leq s_{max}$, we define the odd function $\mathcal{M}_e(s)$ using eqn (11). The iteration algorithm described in section II.B is used to restore the signal from 0 to s_a . In this work, the band-pass filter that selects signal with the range $r_1 < r < r_2$ in the real space region is given by

$$\mathcal{H}(r) = e^{-\left(\frac{r-r_c}{w}\right)^{2N}}, \quad (16)$$

where $r_c = (r_1 + r_2)/2$ and $w = (r_2 - r_1)/2$. The sharpness of the filter is determined by the integer number $N > 0$. The parameters of $\mathcal{H}(r)$ are determined by prior knowledge of the studied molecule, giving the minimum and maximum of the interatomic distances. The parameter r_1 should be a bit smaller than the minimum interatomic distance, and r_2 a bit larger than the maximum interatomic distance.

A. Trifluoroiodomethane

We have first tested the iterative algorithm to restore the electron diffraction signal in the missing region with a small molecule trifluoroiodomethane (CF_3I). We have applied the algorithm to the static diffraction signal $sM(s)$ and the signal of the changed molecular structure $\Delta sM(s)$ to retrieve the missing signal from 0 to 2\AA^{-1} . In this section, the damping constant is $d = 0.01\text{\AA}^2$, and the filter parameter $N = 20$. In APPENDIX C, we applied the iterative algorithm to retrieve the simulated X-ray diffraction signal, where the useful data in practical X-ray experiments is usually from around 0.5\AA^{-1} to 4.5\AA^{-1} [2, 51, 52]. We demonstrated that the missing X-ray signal from 0\AA^{-1} to 1\AA^{-1} can be recovered using the available signal from 1\AA^{-1} to 4\AA^{-1} .

1. Static diffraction

The structure of a CF_3I molecule [53] is shown in figure 2(a), where the iodine atom is purple, the carbon is grey, and the fluorine atoms are green. The interatomic distances of the CF_3I molecule are $r_{\text{CF}} =$

1.33\AA , $r_{\text{CI}} = 2.14\text{\AA}$, $r_{\text{FF}} = 2.15\text{\AA}$ and $r_{\text{FI}} = 2.89\text{\AA}$. The $\mathcal{M}(s)$, which is identical to the $sM(s)$ for $s \geq 0$, is calculated and is shown by the red dashed line in figure 2(a). The blue line in figure 2(a) is $\mathcal{M}_e(s)$, which is the signal with the missing region from 0 to 2\AA^{-1} filled by a linear function given by eqn (11). We used $\mathcal{M}_e(s)$ as $\tilde{\mathcal{M}}_1(s)$ for the 1st iteration and applied the Fourier sine transform to produce $\mathcal{P}_1(r)$, which is shown as the blue line in figure 2(b). In figure 2(b), $\mathcal{P}(r)$, which is the Fourier sine transform of $\mathcal{M}(s)$, is the red dashed line for comparison, and the green line is the band-pass filter $\mathcal{H}(r)$ with parameters $r_1 = 1\text{\AA}$, $r_2 = 3.4\text{\AA}$.

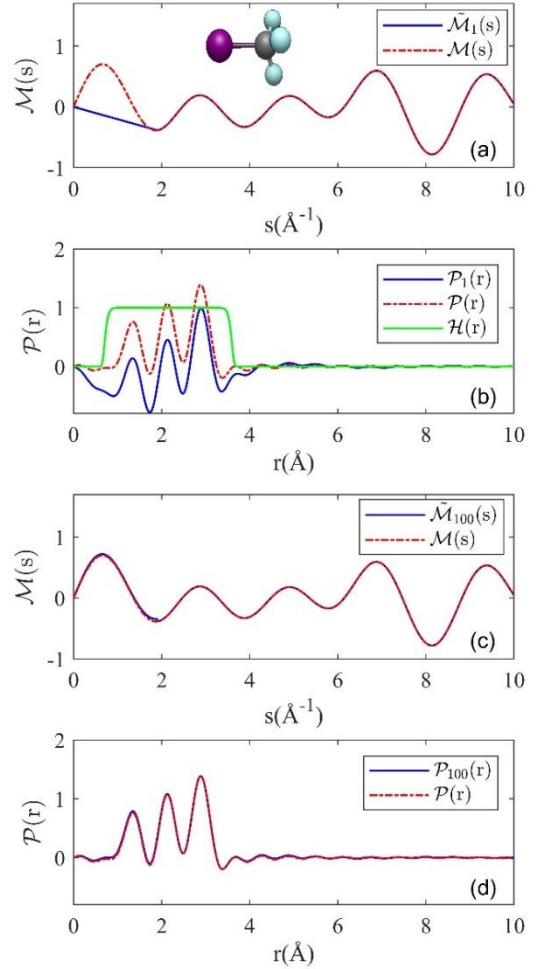


Figure 2. Restoring the missing simulated diffraction data of CF_3I . (a) $\tilde{\mathcal{M}}_1(s)$ is the signal with the missing region from 0 to 2\AA^{-1} , which is filled by the blue solid line and is the input for the 1st iteration. The calculated signal without the missing region, $\mathcal{M}(s)$, is the red dashed line, used as a reference for comparison. The inset is the structure of a CF_3I molecule, where the iodine atom is purple, the carbon atom is grey, and the fluorine atoms are green. (b) The Fourier sine

transform of $\tilde{\mathcal{M}}_1(s)$ and $\mathcal{M}(s)$ are the blue and red dashed lines, denoted as $\mathcal{P}_1(r)$ and $\mathcal{P}(r)$, respectively. The band-pass filter $\mathcal{H}(r)$ is the green line. (c) The restored signal after 100 iterations, denoted as $\tilde{\mathcal{M}}_{100}(s)$, shown by the blue line. The red dashed line is $\mathcal{M}(s)$. (d) The Fourier transform of $\tilde{\mathcal{M}}_{100}(s)$ produces $\mathcal{P}_{100}(r)$ plotted with the blue line. The red dashed line is $\mathcal{P}(r)$.

There is an obvious artifact $\mathcal{A}(r)$ in $\mathcal{P}_1(r)$ compared to $\mathcal{P}(r)$, which makes part of $\mathcal{P}_1(r)$ negative, whereas the PDF of the static diffraction signal of a molecule should be non-negative ($\mathcal{P}(r) \geq 0$). In the case of the static diffraction signal, the artifact term $\mathcal{A}(r)$ can be estimated by the values at the negative valleys and therefore be corrected. However, this method can only be applied to correct the artifacts when we know that $\mathcal{P}(r) \geq 0$ or $\mathcal{P}(r) \leq 0$, and it cannot be used to correct the $\mathcal{A}(r)$ term when $\mathcal{P}(r)$ can be both positive and negative. Here we have used the iterative algorithm described in section II.B to retrieve the signal from 0 to 2\AA^{-1} . After 100 iterations, we have obtained $\tilde{\mathcal{M}}_{100}(s)$ and $\mathcal{P}_{100}(r)$, which are shown by the blue lines in figure 2(c) and 2(d) respectively. The difference between $\tilde{\mathcal{M}}_{100}(s)$ and $\mathcal{M}(s)$ is significantly reduced, and the restored data from 0 to 2\AA^{-1} is in good agreement with the originally calculated signal $\mathcal{M}(s < 2\text{\AA}^{-1})$.

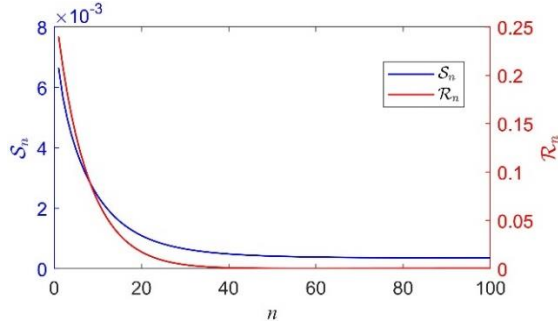


Figure 3. \mathcal{S}_n and \mathcal{R}_n , as functions of iteration number, in retrieving the static CF_3I scattering signal. The iteration number is denoted as n .

For the simulated signal, the sum of squared residuals is defined to check the accuracy of the restored signal $\tilde{\mathcal{M}}_n(s)$ from 0 to 2\AA^{-1} compared to the original signal $\mathcal{M}(s)$, given by

$$\mathcal{R}_n = \int_0^{s_a} [\tilde{\mathcal{M}}_n(s) - \mathcal{M}(s)]^2 dr / s_a. \quad (17)$$

\mathcal{S}_n and \mathcal{R}_n are calculated for static CF_3I scattering data, shown in figure 3. Note that the left y axis is for \mathcal{S}_n , and right y axis for \mathcal{R}_n . Both \mathcal{S}_n and \mathcal{R}_n converge in a similar way and approach a small value that is close to zero after 50 iterations, which indicates the

signal from 0 to 2\AA^{-1} is successfully restored through the iterative algorithm.

2. Elongation of CI distance in CF_3I

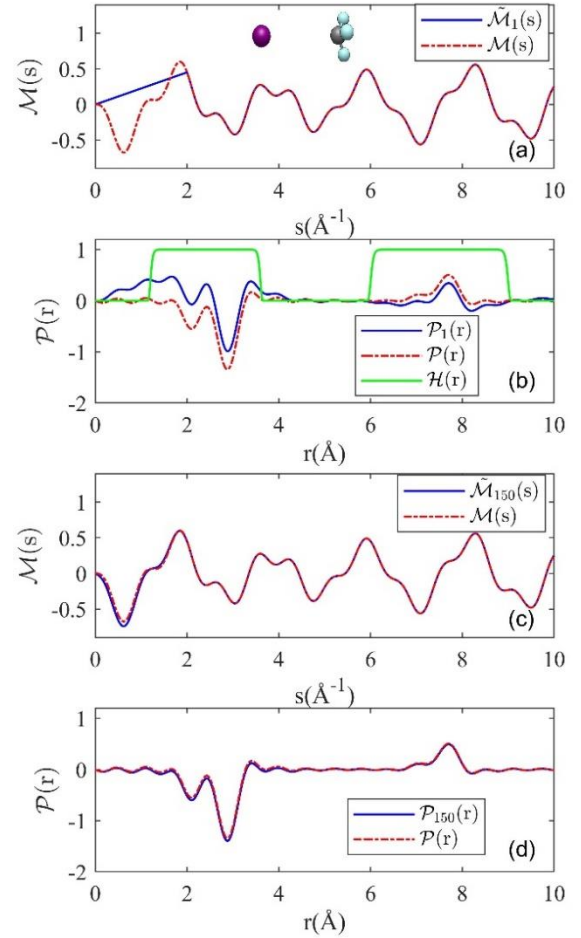


Figure 4. Restoring the simulated diffraction data of CF_3I from 0 to 2\AA^{-1} , where the CI distance of CF_3I molecule is elongated by 5\AA . (a) $\tilde{\mathcal{M}}_1(s)$ is the signal with the missing region from 0 to 2\AA^{-1} , plotted with the blue line and is the input signal for the 1st iteration. The calculated signal without the missing region, $\mathcal{M}(s)$, is the red dashed line. (b) The Fourier sine transform of $\tilde{\mathcal{M}}_1(s)$ and $\mathcal{M}(s)$ are the blue and red dashed lines, denoted as $\mathcal{P}_1(r)$ and $\mathcal{P}(r)$, respectively. The band-pass filter $\mathcal{H}(r)$ is the green line. (c) The restored signal after 150 iterations, denoted as $\tilde{\mathcal{M}}_{150}(s)$, is shown by the blue line. The red dashed line is $\mathcal{M}(s)$. (d) The Fourier transform of $\tilde{\mathcal{M}}_{150}(s)$ produces $\mathcal{P}_{150}(r)$, shown in the blue line. The red dashed is $\mathcal{P}(r)$.

In this section, we simulated the electron diffraction signal of CF_3I with CI distance increased by 5\AA , denoted as $\Delta\text{CI} = 5\text{\AA}$ below, and the CF_3 structure remains unchanged. We have calculated the

diffraction-difference intensity, formulated as $\Delta I_M(s) = I_M(s, \Delta \text{CI} = 5\text{\AA}) - I_M^0(s)$, where $I_M^0(s)$ is the molecular scattering of CF_3I in the ground state. The $\Delta sM(s)$ is calculated using eqn (7), and the $\mathcal{M}(s)$ is defined with eqn (8). In this case, some of the $c_{jk}(s)$ terms in eqn (8) are negative, indicating the loss of interatomic distances, whereas the other $c_{jk}(s)$ terms are positive, corresponding to the newly generated interatomic distances compared to the unexcited molecules. We used eqn (11) to define $\mathcal{M}_e(s)$ with $\Delta sM(s)$ from 2\AA^{-1} to 10\AA^{-1} . In the 1st iteration, we set $\tilde{\mathcal{M}}_1(s) = \mathcal{M}_e(s)$. In figure 4 (a), the $\tilde{\mathcal{M}}_1(s)$ from 0 to 10\AA^{-1} is shown by the blue line, whereas the original calculated signal $\mathcal{M}(s)$ is the red dashed line used as a reference for comparison.

The $\mathcal{P}_1(r)$, which corresponds to the blue line in figure 4(b), is produced by the Fourier sine transform of $\tilde{\mathcal{M}}_1(s)$. In $\mathcal{P}_1(r)$, the two valleys at 2.14\AA and 2.89\AA are due to the loss of the two interatomic distance r_{CI} and r_{FI} of CF_3I in the ground state. Due to the CI elongation by 5\AA , the newly generated interatomic distance of CI and FI are the two peaks around 7\AA and 7.7\AA , respectively. These signals, although they contain artifacts, can be used as the prior knowledge to define the band-pass filter, given by

$$\mathcal{H}(r) = \mathcal{H}_1(r) + \mathcal{H}_2(r), \quad (18)$$

where both $\mathcal{H}_1(r)$ and $\mathcal{H}_2(r)$ are given by eqn (16). For $\mathcal{H}_1(r)$, $r_1 = 1.6\text{\AA}$, $r_2 = 3.6\text{\AA}$; and for $\mathcal{H}_2(r)$, $r_1 = 6.5\text{\AA}$, $r_2 = 8.5\text{\AA}$. The band-pass filter $\mathcal{H}(r)$ is the green line, and $\mathcal{P}(r)$ is the red dashed line in figure 4(b).

After 150 iterations, we obtained $\tilde{\mathcal{M}}_{150}(s)$ and $\mathcal{P}_{150}(r)$, which are shown by the blue lines in figure 4(c) and 4(d) respectively. $\mathcal{M}(s)$ and $\mathcal{P}(r)$, which correspond to the original signal without the missing region, are the red dashed lines in figure 4(c) and 4(d). The difference between $\tilde{\mathcal{M}}_{150}(s)$ and $\mathcal{M}(s)$ is significantly reduced, and the restored data from 0 to 2\AA^{-1} is in good agreement to the originally calculated signal $\mathcal{M}(s < 2\text{\AA}^{-1})$. The $\mathcal{P}_{150}(r)$ and $\mathcal{P}(r)$ are in good agreement as well.

\mathcal{S}_n and \mathcal{R}_n are calculated with eqn (15) and eqn (17), respectively, shown in figure 5. Note that the left y axis is for \mathcal{S}_n , and right y axis for \mathcal{R}_n . Both \mathcal{S}_n and \mathcal{R}_n approach to zero after 50 iterations, which indicates the signal from 0 to 2\AA^{-1} is successfully restored through the iterative algorithm.

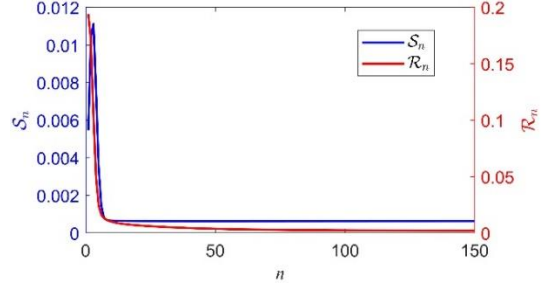


Figure 5. \mathcal{S}_n and \mathcal{R}_n , as functions of iteration number, in retrieving the simulated CF_3I scattering data with C-I elongated by 5\AA . The iteration number is denoted as n .

B. Iodobenzene

It is more challenging to restore the scattering signal in the missing region for bigger molecules since the PDFs of such molecules have broader distributions, which makes it challenging to remove the artifacts through a band-pass filter. In this section, we have tested the iterative algorithm with the static diffraction signal of iodobenzene ($\text{C}_6\text{H}_5\text{I}$) [54]. The damping constant is $d = 0.01\text{\AA}^2$, and the filter parameter $\mathcal{N} = 15$.

1. Static diffraction

The structure of iodobenzene is shown in figure 6(a), in which the carbon atoms are represented by dark grey color, the iodine atom is purple color, and the hydrogen atoms by light grey color. The minimum and maximum interatomic distances in iodobenzene are 1.090\AA and 5.953\AA . We defined the band-pass filter $\mathcal{H}(r)$, given by eqn (16), with parameters $r_1 = 0.68\text{\AA}$, $r_2 = 6.20\text{\AA}$. The input and restored signals are shown in figure 6. The $\tilde{\mathcal{M}}_1(s)$ and $\mathcal{M}(s)$ correspond to the blue solid and red dashed lines in figure 6(a). The missing region in $\tilde{\mathcal{M}}_1(s)$ from 0 to 1.7\AA^{-1} is filled with a linear function, and the available signal is from 1.7\AA^{-1} to 10\AA^{-1} . The $\mathcal{P}_1(r)$ and $\mathcal{P}(r)$, which are the Fourier sine transforms of $\tilde{\mathcal{M}}_1(s)$ and $\mathcal{M}(s)$, correspond to the blue solid and red dashed lines in figure 6(b). Significant artifacts were introduced into $\mathcal{P}_1(r)$ due to the filled data in the missing region of $\tilde{\mathcal{M}}_1(s)$. The band pass filter $\mathcal{H}(r)$ corresponds to the green solid line in figure 6(b). After 120 iterations, we obtained $\tilde{\mathcal{M}}_{120}(s)$ and $\mathcal{P}_{120}(r)$, which are shown by the blue solid lines in figure 6(c) and 6(d) respectively. The difference between $\tilde{\mathcal{M}}_{120}(s)$ and $\mathcal{M}(s)$ is significantly reduced compared to the difference between $\tilde{\mathcal{M}}_1(s)$ and $\mathcal{M}(s)$. The retrieved $\tilde{\mathcal{M}}_{120}(s)$ is in good agreement to $\mathcal{M}(s)$.

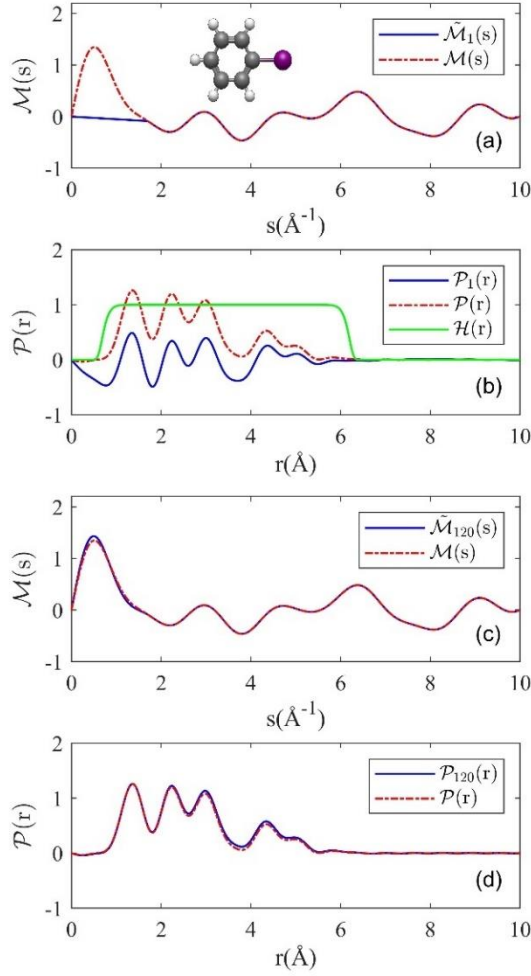


Figure 6. Retrieving the static diffraction of iodobenzene. (a) $\tilde{\mathcal{M}}_1(s)$ is the signal with the missing region from 0 to 1.7\AA^{-1} , which is the blue solid line. The original signal $\mathcal{M}(s)$ is the red dashed line. The inset shows the structure of iodobenzene, where the carbon atoms are dark grey color, the iodine atom is purple color, and the hydrogen atoms are light grey color. (b) The Fourier sine transform of $\tilde{\mathcal{M}}_1(s)$ and $\mathcal{M}(s)$ produce $\mathcal{P}_1(r)$ and $\mathcal{P}(r)$, corresponding to the blue and red dashed lines, respectively. The band-pass filter $\mathcal{H}(r)$ is the green line. (c) The restored signal after 120 iterations, $\tilde{\mathcal{M}}_{120}(s)$, is shown by the blue line. The red dashed line is $\mathcal{M}(s)$. (d) The Fourier transform of $\tilde{\mathcal{M}}_{120}(s)$ produces $\mathcal{P}_{120}(r)$, shown in the blue line. The red dashed is $\mathcal{P}(r)$.

The \mathcal{S}_n and \mathcal{R}_n are calculated with eqn (15) and eqn (17) for retrieving the static diffraction of iodobenzene, shown in figure 7. Note that the left y axis is for \mathcal{S}_n , and right y axis for \mathcal{R}_n . The inset highlights \mathcal{S}_n and \mathcal{R}_n approaching to a small value, whereas \mathcal{R}_n converges much slower than \mathcal{S}_n . Both \mathcal{S}_n and

\mathcal{R}_n approach a small value that is close to zero after 80 iterations.

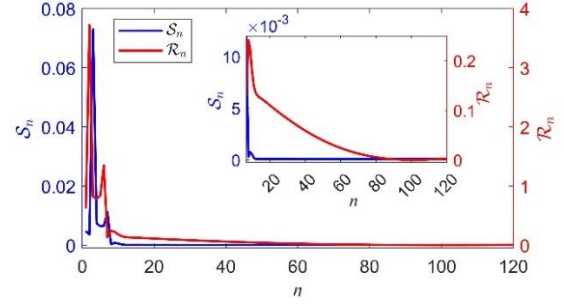


Figure 7. Functions \mathcal{S}_n and \mathcal{R}_n in retrieving the static diffraction of iodobenzene.

2. CI bond breaking

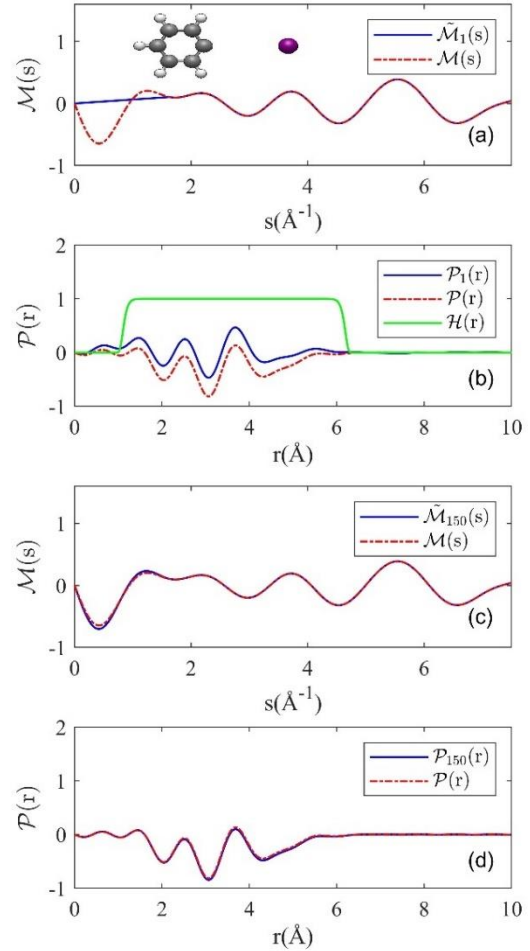


Figure 8. Retrieving the diffraction signal of dissociated iodobenzene from 0 to 1.63\AA^{-1} . (a) $\tilde{\mathcal{M}}_1(s)$ is the signal with the missing region from 0 to 1.63\AA^{-1} , which is the blue solid line. The original signal $\mathcal{M}(s)$ is the red dashed line. The inset shows the structure of dissociated iodobenzene, where the

carbon atoms are dark grey color, the iodine atom is purple color, and the hydrogen atoms are light grey color. The CI bond breaking indicates that the distance between the phenyl ring and iodine atom is ∞ . (b) The Fourier sine transform of $\tilde{\mathcal{M}}_1(s)$ and $\mathcal{M}(s)$ produce $\mathcal{P}_1(r)$ and $\mathcal{P}(r)$, corresponding to the blue and red dashed lines, respectively. The band-pass filter $\mathcal{H}(r)$ is the green line. (c) The restored signal after 150 iterations, $\tilde{\mathcal{M}}_{150}(s)$, is shown by the blue line. The red dashed line is $\mathcal{M}(s)$. (d) The Fourier transform of $\tilde{\mathcal{M}}_{150}(s)$ produces $\mathcal{P}_{150}(r)$, shown in the blue line. The red dashed is $\mathcal{P}(r)$.

Now we simulated the electron diffraction signal of dissociated iodobenzene with CI bond cleavage, and the structure of phenyl ring remains unchanged. We have calculated the diffraction-difference intensity, formulated as $\Delta I_M(s) = I_{C_6H_5}(s) + I_I(s) - I_{C_6H_5I}(s)$, where $I_{C_6H_5}(s)$, $I_I(s)$, $I_{C_6H_5I}(s)$ are the molecular scattering intensities of the phenyl ring, an iodine atom and iodobenzene in the ground state calculated with eqn (3). The $\Delta sM(s)$ is calculated using eqn (7), and the $\mathcal{M}(s)$ is defined with eqn (8). We used eqn (11) to define $\mathcal{M}_e(s)$ with $\Delta sM(s)$ from 1.63 \AA^{-1} to 7.5 \AA^{-1} . In the 1st iteration, we set $\tilde{\mathcal{M}}_1(s) = \mathcal{M}_e(s)$. In figure 8 (a), the $\tilde{\mathcal{M}}_1(s)$ from 0 to 7.5 \AA^{-1} is shown by the blue line, whereas the original calculated signal $\mathcal{M}(s)$ is the red dashed line used as a reference for comparison. The $\mathcal{P}_1(r)$, which corresponds to the blue line in figure 8(b), is produced by the Fourier sine transform of $\tilde{\mathcal{M}}_1(s)$. We defined the band-pass filter $\mathcal{H}(r)$, given by eqn (16), with parameters $r_1 = 1.10 \text{ \AA}$, $r_2 = 6.20 \text{ \AA}$. The band-pass filter $\mathcal{H}(r)$ is the green line, and $\mathcal{P}(r)$ is the red dashed line in figure 8(b).

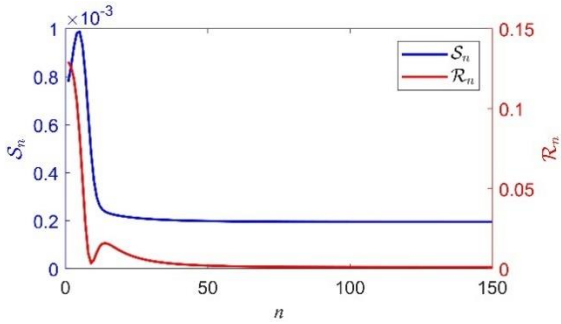


Figure 9. Functions \mathcal{S}_n and \mathcal{R}_n in retrieving the scattering signal of dissociated iodobenzene. the iteration number is denoted as n .

After 150 iterations, we obtained $\tilde{\mathcal{M}}_{150}(s)$ and $\mathcal{P}_{150}(r)$, which are shown by the blue lines in figure 8(c) and 8(d) respectively. $\mathcal{M}(s)$ and $\mathcal{P}(r)$, which correspond to the original signal without the missing region, are the red dashed lines in figure 8(c) and 8(d). The difference between $\tilde{\mathcal{M}}_{150}(s)$ and $\mathcal{M}(s)$ is

significantly reduced, and the restored data from 0 to 1.63 \AA^{-1} is in good agreement to the originally calculated signal $\mathcal{M}(s < 1.63 \text{ \AA}^{-1})$. The $\mathcal{P}_{150}(r)$ and $\mathcal{P}(r)$ are in good agreement as well. \mathcal{S}_n and \mathcal{R}_n are calculated with eqn (15) and eqn (17) for retrieving the diffraction signal of dissociated iodobenzene, shown in figure 9. Note that the left y axis is for \mathcal{S}_n , and right y axis for \mathcal{R}_n . Both \mathcal{S}_n and \mathcal{R}_n approach zero after 80 iterations.

IV. APPLICATION TO EXPERIMENTAL DATA

The iterative algorithm has been demonstrated to successfully restore the signal in the missing region for the simulated diffraction signals which are free of noise and artifacts. However, in UED experiments, UED signals contain noise, artifacts and backgrounds that are added to the signal. In this section, we have applied the iterative algorithm to retrieve the experimental static diffraction signal and laser induced dissociation signal of the CF_3I and iodobenzene molecules.

The experiment was conducted using a table-top keV-UED instrument, which has been described in detail previously [3, 4, 7]. More details of the experiment are available in APPENDIX A. Briefly, a femtosecond ultraviolet (UV) laser pulse (the pump) triggers a photoinduced dissociation of the sample molecules (CF_3I or iodobenzene), and a femtosecond electron pulse (the probe) is used to interrogate the molecules. The relative time delay between the laser and electron pulses is adjusted by an optical delay line. The time zero of the signal is defined as the time delay when the first changes in the ΔsM signal become visible.

A. Static diffraction

The static diffraction patterns are recorded by setting the time delay to be negative ($t < 0$), such as -1 ps, which indicates that the arrival of the electron pulse is before the laser pulse. Therefore, the scattering signal of the unexcited molecules is recorded. The 2D static diffraction patterns from sample molecules are azimuthally averaged to obtain the 1-D $I_{total}(s)$. The zeros of the calculated sM are used to fit and remove a background from the experimental $I_{total}(s)$, allowing us to obtain the experimental $I_M(s)$ [5, 44]. The removed background consists of atomic scattering, other experimental background scattering and noise. Eqn (4) is used to calculate the $sM(s)$ for the static diffraction signal.

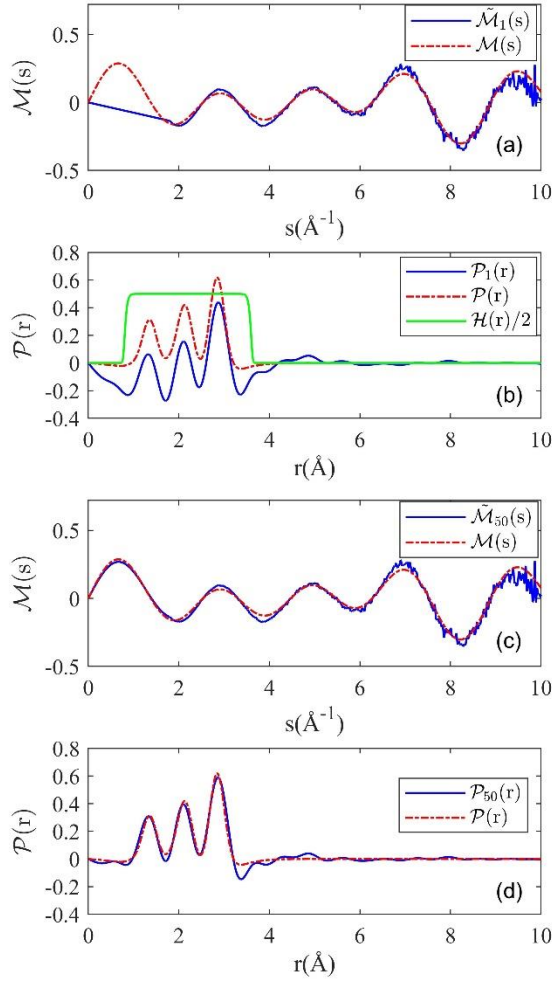


Figure 10. Retrieving experimental static diffraction of CF_3I from 0 to 1.8\AA^{-1} . (a) $\tilde{\mathcal{M}}_1(s)$ is the blue solid line. The $\mathcal{M}(s)$ is the red dashed line. (b) $\mathcal{P}_1(r)$ and $\mathcal{P}(r)$ correspond to the blue and red dashed lines, respectively. The filter function $\mathcal{H}(r)$ is the green line. (c) The restored signal after 50 iterations, $\tilde{\mathcal{M}}_{50}(s)$, is shown by blue line. The red dashed line is $\mathcal{M}(s)$. (d) The $\mathcal{P}_{50}(r)$ is the blue line, and $\mathcal{P}(r)$ is red dashed line.

First, we applied the algorithm to retrieve signal at missing region in experimental static diffraction signal of CF_3I . Figure 10(a) shows the theoretical static signal $\mathcal{M}(s)$ (red dashed line) calculated with the structure of CF_3I in the ground state, and the experimental static signal $\tilde{\mathcal{M}}_1(s)$ of CF_3I (blue solid line) with the available data from 1.8\AA^{-1} to 10\AA^{-1} , where the missing region is filled with a linear function described in eqn (11). Note that the calculated signal $\mathcal{M}(s)$ is pictured only for reference and is not used to retrieve the missing region of the experimental signal. $\mathcal{P}_1(r)$ and $\mathcal{P}(r)$, which are the Fourier sine

transforms of $\tilde{\mathcal{M}}_1(s)$ and $\mathcal{M}(s)$, correspond to the blue solid and red dashed lines in figure 10(b). The band-pass filter $\mathcal{H}(r)$ with parameters $r_1 = 0.8\text{\AA}$, $r_2 = 3.6\text{\AA}$ corresponds to the green solid line in figure 10(b). After 50 iterations, we obtained $\tilde{\mathcal{M}}_{50}(s)$ and $\mathcal{P}_{50}(r)$, which are shown by the blue solid lines in figure 10(c) and 10(d) respectively. The retrieved diffraction signal $\tilde{\mathcal{M}}_{50}(s)$ and its transform $\mathcal{P}_{50}(r)$ are in good agreement to the calculated diffraction signal $\mathcal{M}(s)$ and $\mathcal{P}(r)$.

Note that the theoretical signal $\mathcal{M}(s)$ can be calculated with the structure of the molecule for static diffraction, whereas in general experiments, such as time-resolved experiments, the $\mathcal{M}(s)$ usually is not available as the accurate molecular structure is unknown after laser excitation. Therefore, \mathcal{R}_n cannot be defined accordingly. Figure 11 shows \mathcal{S}_n as a function of iteration number calculated with eqn (15) for retrieving the experimental static signal of CF_3I . The function \mathcal{S}_n decreases monotonically as n increases and converges to 6×10^{-4} .

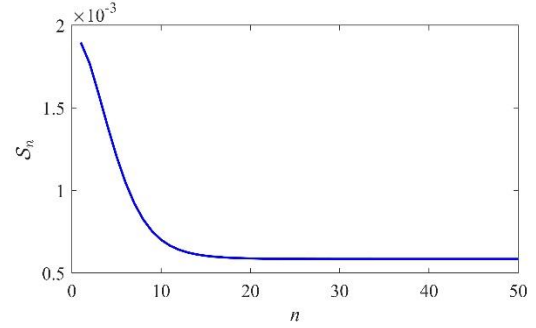


Figure 11. The function \mathcal{S}_n in retrieving the static diffraction of CF_3I . The iteration number is denoted as n .

Now we apply the iterative algorithm to restore the signal at missing region in experimental static diffraction signal of iodobenzene molecules. Figure 12(a) shows the theoretical static signal $\mathcal{M}(s)$ (red dashed line) calculated with the structure of iodobenzene in the ground state [54], and the experimental static signal $\tilde{\mathcal{M}}_1(s)$ of iodobenzene (blue solid line) with the available data from 1.7\AA^{-1} to 10\AA^{-1} , where the missing region is filled with a linear function described in eqn (11). The $\mathcal{P}_1(r)$ and $\mathcal{P}(r)$, which are the Fourier sine transforms of $\tilde{\mathcal{M}}_1(s)$ and $\mathcal{M}(s)$, correspond to the blue solid and red dashed lines in figure 12(b). Significant artifacts are introduced in the $\mathcal{P}_1(r)$ due to the filling of the linear function in the missing region. The range of interatomic distances in iodobenzene is from 1.090\AA to 5.953\AA . Therefore, we define the band pass filter $\mathcal{H}(r)$ with parameters $r_1 = 0.68\text{\AA}$, $r_2 = 6.20\text{\AA}$, which

corresponds to the green solid line in figure 12(b). After 120 iterations, we obtained $\tilde{\mathcal{M}}_{120}(s)$ and $\mathcal{P}_{120}(r)$, which are shown by the blue solid lines in figure 12(c) and 12(d) respectively. The retrieved diffraction signal $\tilde{\mathcal{M}}_{120}(s)$ and its transform $\mathcal{P}_{120}(r)$ are in good agreement to the calculated diffraction signal $\mathcal{M}(s)$ and $\mathcal{P}(r)$.

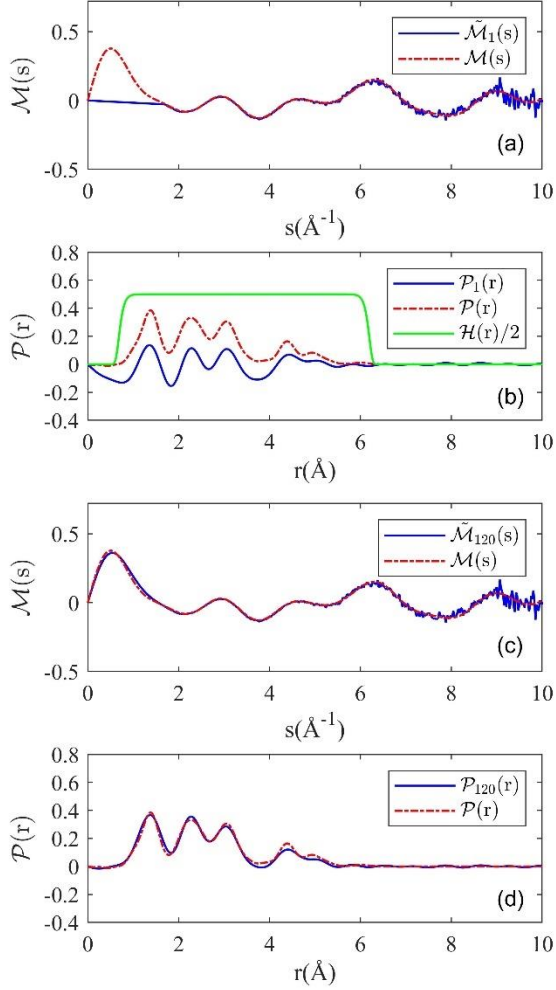


Figure 12. Retrieving experimental static diffraction of iodobenzene from 0 to 1.7\AA^{-1} . (a) $\tilde{\mathcal{M}}_1(s)$ is the signal with the missing region from 0 to 1.7\AA^{-1} , which is the blue solid line. The calculated static diffraction signal $\mathcal{M}(s)$ is the red dashed line. (b) $\mathcal{P}_1(r)$ and $\mathcal{P}(r)$ correspond to the blue solid and red dashed lines, respectively. The band-pass filter $\mathcal{H}(r)$ is the green line. (c) The restored signal after 120 iterations, $\tilde{\mathcal{M}}_{120}(s)$, is shown by blue line. The red dashed line is $\mathcal{M}(s)$. (d) $\mathcal{P}_{120}(r)$ is the blue line, and $\mathcal{P}(r)$ is the red dashed line.

Figure 13 shows the calculated \mathcal{S}_n , as a function of iteration number, for retrieving the experimental static

signal of iodobenzene molecules. The \mathcal{S}_n fluctuates in the first ten iterations and converges to 3×10^{-4} after 20 iterations. The behavior of \mathcal{S}_n is similar to the case of retrieving simulated static diffraction signal of iodobenzene, shown in figure 7. This behavior is attributed to the broad distribution of PDF.

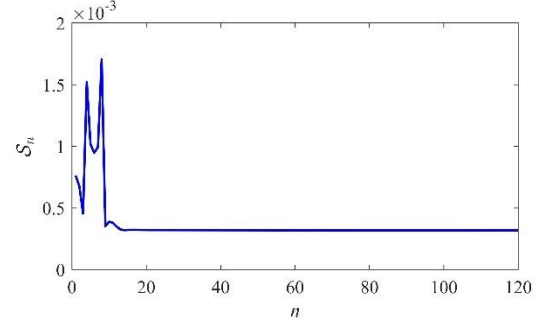


Figure 13. The function \mathcal{S}_n in retrieving the static diffraction of iodobenzene molecules. The iteration number is denoted as n .

B. Diffraction signal of dissociated molecules

We now apply the iterative algorithm to restore the missing region in the diffraction signal from photo-dissociated molecules, including CF_3I and iodobenzene. We used a femtosecond 266 nm laser to excite the sample molecules to the A-band (more experimental details in APPENDIX A), promoting a non-bonding (n) electron from the iodine atom valence shell to the σ^* anti-bonding orbital of the CI bond [55-62]. The UV excitation of the molecules, including CF_3I and iodobenzene, leads to a rapid cleavage of the CI bond. The pump-probe diffraction patterns are recorded as a function of time delays, and the time zero ($t=0$) is defined when the dissociation signal starts. The diffraction signals with negative time delays are used as a reference, which contains the diffraction signals of the unexcited molecules and other background signals, such as scattered laser light and background electrons. Eqn (6) and (7) are used to calculate the ΔsM in the photo-dissociation experiment of CF_3I (more details in APPENDIX B).

First, we present the retrieval result of diffraction signals from photo-dissociated CF_3I molecules. The signal $\tilde{\mathcal{M}}_1(s)$, shown in figure 14(a), is the average of the experimental ΔsM from 0.2ps to 2 ps. The available signal is from 1.8 to 10\AA^{-1} . Significant noise appears in the experimental data. We have used a simple model to approximate the comparable dissociation signal, in which after UV excitation the distance between the iodine atom and CF_3 radical is infinite, and the structure of the CF_3 fragment remains unchanged, whereas in reality we expect the CF_3 fragment to be vibrationally excited and associated

with new equilibrium positions. Using this simple model, the diffraction-difference intensity for CF_3I dissociation is given by $\Delta I_M(s) = I_{\text{CF}_3}(s) + I_I(s) - I_{\text{CF}_3\text{I}}(s)$, where $I_{\text{CF}_3}(s)$, $I_I(s)$, $I_{\text{CF}_3\text{I}}(s)$ are the molecular scattering intensities of CF_3 , an iodine atom and CF_3I calculated with eqn (3). The ΔsM of this simple model is calculated by eqn (7), which is represented by $\mathcal{M}(s)$ and is shown by the red dashed line in figure 14 (a). A good agreement is achieved in the available experimental s ranging from 1.8 to 10\AA^{-1} .

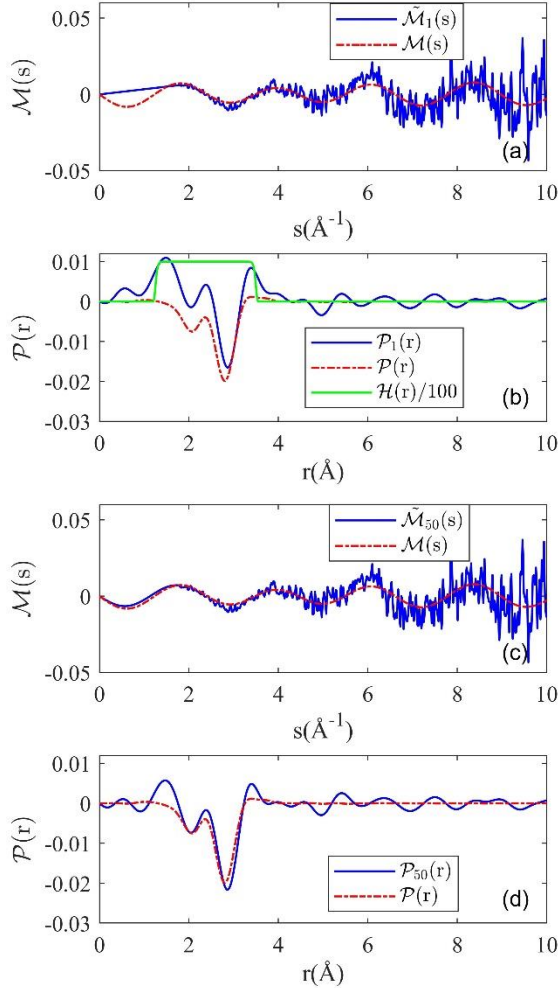


Figure 14. Retrieving the diffraction signal of photo-dissociated CF_3I molecules. (a) $\tilde{\mathcal{M}}_1(s)$ is the signal with the missing region from 0 to 1.8\AA^{-1} , which is the blue solid line. The $\mathcal{M}(s)$ based on the simple model is the red dashed line. (b) The Fourier sine transform of $\tilde{\mathcal{M}}_1(s)$ and $\mathcal{M}(s)$ produce $\mathcal{P}_1(r)$ and $\mathcal{P}(r)$, corresponding to the blue and red dashed lines, respectively. The band-pass filter $\mathcal{H}(r)$ is the green line. (c) The restored signal after 50 iterations, $\tilde{\mathcal{M}}_{50}(s)$, is shown by blue line. The red dashed line is $\mathcal{M}(s)$. (d)

The Fourier transform of $\tilde{\mathcal{M}}_{50}(s)$ produces $\mathcal{P}_{50}(r)$, shown in the blue line. The red dashed is $\mathcal{P}(r)$.

$\mathcal{P}_1(r)$ and $\mathcal{P}(r)$, which are the Fourier sine transforms of $\tilde{\mathcal{M}}_1(s)$ and $\mathcal{M}(s)$, correspond to the blue solid and red dashed lines in figure 14(b). The band pass filter $\mathcal{H}(r)$ with parameters $r_1 = 1.25\text{\AA}$, $r_2 = 3.5\text{\AA}$ corresponds to the green solid line in figure 10(b). After 50 iterations, we obtained $\tilde{\mathcal{M}}_{50}(s)$ and $\mathcal{P}_{50}(r)$, which are shown by the blue solid lines in figure 10(c) and 14(d) respectively. The retrieved diffraction signal $\tilde{\mathcal{M}}_{50}(s)$ from 0 to 1.8\AA^{-1} is in good agreement to the calculated diffraction signal $\mathcal{M}(s)$ based on the simple model. Figure 15 shows \mathcal{S}_n as a function of iteration number calculated with eqn (15) in retrieving the photo-dissociation signal of CF_3I .

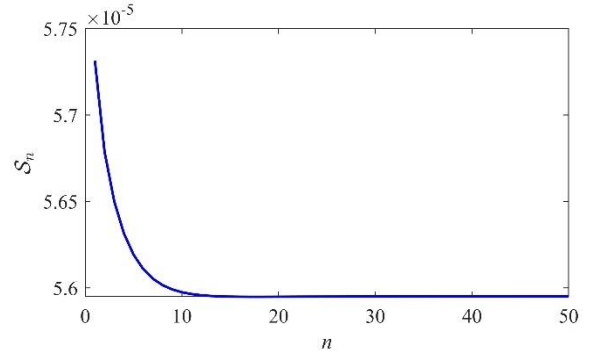


Figure 15. The function \mathcal{S}_n computed in retrieving the photo-dissociation signal of CF_3I . The iteration number is denoted as n .

Now we demonstrated application of the iterative algorithm to the diffraction signals from photo-dissociated iodobenzene molecules. The signal $\tilde{\mathcal{M}}_1(s)$ of photo-dissociated iodobenzene, shown in figure 16(a), is the average of the experimental ΔsM from 1ps to 10ps. The available signal is from 1.63 to 7.5\AA^{-1} . Significant noise appears in the experimental data. We have used a simple model to approximate the comparable dissociation signal, in which after UV excitation the distance between the iodine atom and phenyl ring is infinite, and the structure of the phenyl ring remains unchanged, whereas in reality we expect the phenyl ring to be vibrationally excited and associated with new equilibrium positions. The ΔsM of this simple model has been described in section III.B.2, which is represented by $\mathcal{M}(s)$ and is shown by the red dashed line in figure 16 (a). A good agreement is achieved in the available experimental s ranging from 1.63 to 7.5\AA^{-1} . $\mathcal{P}_1(r)$ and $\mathcal{P}(r)$, which are the Fourier sine transforms of $\tilde{\mathcal{M}}_1(s)$ and $\mathcal{M}(s)$, correspond to the blue solid and red dashed lines in figure 16(b). The band pass filter $\mathcal{H}(r)$ with parameters $r_1 = 0.75\text{\AA}$, $r_2 = 6.00\text{\AA}$ corresponds to the

green solid line in figure 16(b). After 150 iterations, we obtained $\tilde{\mathcal{M}}_{150}(s)$ and $\mathcal{P}_{150}(r)$, which are shown by the blue solid lines in figure 16(c) and 16(d) respectively. The retrieved diffraction signal $\tilde{\mathcal{M}}_{150}(s)$ from 0 to 1.63 \AA^{-1} is in good agreement to the calculated diffraction signal $\mathcal{M}(s)$ based on the simple model.

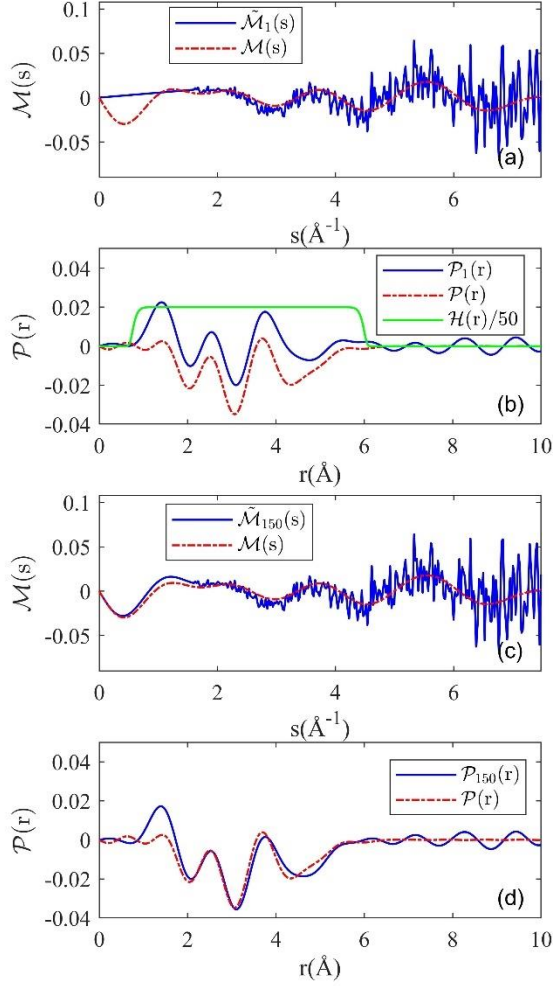


Figure 16. Retrieving the diffraction signal of photo-dissociated iodobenzene molecules. (a) $\tilde{\mathcal{M}}_1(s)$ is the signal with the missing region from 0 to 1.63 \AA^{-1} , which is the blue solid line. The $\mathcal{M}(s)$ based on the simple model is the red dashed line. (b) The Fourier sine transform of $\tilde{\mathcal{M}}_1(s)$ and $\mathcal{M}(s)$ produce $\mathcal{P}_1(r)$ and $\mathcal{P}(r)$, corresponding to the blue and red dashed lines, respectively. The band-pass filter $\mathcal{H}(r)$ is the green line. (c) The restored signal after 150 iterations, $\tilde{\mathcal{M}}_{150}(s)$, is shown by blue line. The red dashed line is $\mathcal{M}(s)$. (d) The Fourier transform of $\tilde{\mathcal{M}}_{150}(s)$ produces $\mathcal{P}_{150}(r)$, shown in the blue line. The red dashed is $\mathcal{P}(r)$.

Figure 17 shows \mathcal{S}_n as a function of iteration number calculated with eqn (15) in retrieving the photo-dissociation signal of iodobenzene molecules. The \mathcal{S}_n increases in the first 25 iterations and reaches a peak around $n=20$, and then converges to a value below 2.4×10^{-4} after $n=70$.

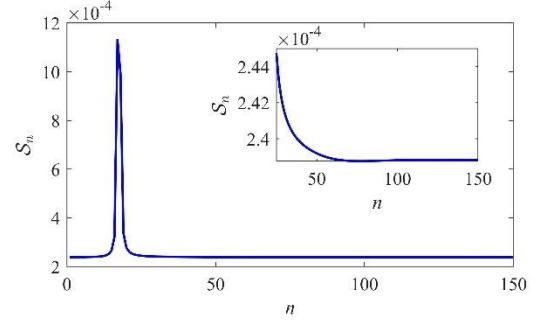


Figure 17. The function \mathcal{S}_n computed in retrieving the photo-dissociation signal of CF_3I . The iteration number is denoted as n .

V. CONCLUSIONS AND DISCUSSIONS

In conclusion, we report an iterative method to restore the electron diffraction signal in the missing region at low momentum transfers using the measurement that is available. The method iteratively transforms back and forth between the sM and the PDF through a Fourier sine transform, applying known constraints in each domain to reduce the artifacts introduced by the data in the missing region until the artifact is minimized. The missing s -range in typical UED experiments is from 0 to a value that is between 1 \AA^{-1} and 2 \AA^{-1} . Using this method, we have successfully restored the simulated diffraction signal of CF_3I and iodobenzene, including static diffraction and signal from changed structures, with a missing s region that matches UED experiments. We then applied the iterative algorithm to experimental diffraction signal of CF_3I and iodobenzamide, for both the static diffraction and photodissociation signals, and successfully restored the data in the missing region.

From the behavior of \mathcal{S}_n and \mathcal{R}_n , we have noticed that both \mathcal{S}_n and \mathcal{R}_n converge in a similar way for small molecules, such as CF_3I . This convergence behavior indicates that the iterative algorithm demonstrates a very good performance for diffraction signals of small molecules since their diffraction signals have a narrow distribution of PDF. However, for bigger molecules like iodobenzene, \mathcal{R}_n converges slower than \mathcal{S}_n , as shown by figure 7 and figure 9. The reason is that the distribution of the PDF signal is broad for big molecules, making more of the artifact term overlap with the PDF, and so it is relatively more challenging to minimize the artifact term. Therefore, the retrieval

method performs better for molecules with a PDF that has a relatively narrow distribution. The convergence behavior of \mathcal{S}_n and \mathcal{R}_n in figure 7 and figure 9 also indicate that the retrieved result could deviate from the true signal even when \mathcal{S}_n reaches a plateau close to zero. Therefore, it is better to have an auxiliary signal, such as the theoretical ΔsM of dissociated CF_3I and iodobenzene based on a simple model, to ensure that the constraints and retrieved results are reasonable.

The iterative algorithm is based on the elastic electron scattering intensity that consists of a series of sinusoidal functions. Therefore, the algorithm in principle can be used to separate the elastic and inelastic scattering signal at the low s -region, such as the UED experimental signal shown in [27, 45].

ACKNOWLEDGMENTS

This work was supported by the US Department of Energy Office of Science, Basic Energy Sciences under award no. DE-SC0014170.

APPENDIX A: EXPERIMENT

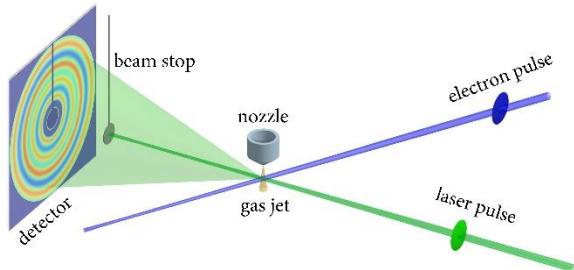


Figure 18. Diagram of the UED experiment. The diagram shows the electron and laser pulses which travel from right to left, and gas jet entering the chamber through a nozzle from the top. A tilted pulse front of the laser pulse is used to compensate for the group velocity mismatch between the laser and electron pulses. A copper beam stop is used to block the directly transmitted electron beam, and the scattered electrons (green cone) are recorded by the detector.

A keV-UED setup is used to capture diffraction patterns from a sample of CF_3I molecules excited by a 266 nm laser pulse as a function of the delay between the pump laser pulse and the probe electron pulses. The diagram of the UED experiment is shown in figure 12. The details of the UED setup have been previously reported in [3, 4, 7, 63, 64]. Each laser pulse (50fs, 800nm, 7mJ) is produced by a Ti: Sapphire laser and is split into two beams with an energy ratio of 9:1, both of which are frequency-tripled to generate 266 nm laser pulses. The repetition rate of the laser is 1kHz.

The higher energy UV pulse is used to pump and dissociate the CF_3I molecules, while the lower energy UV pulse produces an electron pulse as a probe. The full width at half maximum (FWHM) pulse duration of the pump is 120 fs, the maximum pulse energy is 165 μJ and FWHM beam diameter is 200 μm on the sample. The probe electron pulse is produced by shining the weaker UV pulse onto a copper cathode. A hybrid DC-RF electron gun is employed where the electrons are first accelerated to 90 keV (speed of 0.53 c) in a static electric field and then temporally compressed using an RF cavity with a longitudinal time-varying electric field to obtain the minimum temporal pulse duration at the sample. The electron pulse is guided by electron optics and collimated by a 300 μm platinum aperture to deliver a beam current of 8 picoamperes on the sample, corresponding to 50,000 electrons per pulse.

The CF_3I sample (99% purity) was purchased from Sigma Aldrich and was used without further purification in this experiment. The pure CF_3I gas was introduced into the interaction region using a de Laval nozzle with an orifice of 30 μm and a backing pressure of 300 torr. The UV laser pulse energy is 100 μJ for CF_3I experiment to ensure the one-photon excitation range. The iodobenzene sample was purchased from Millipore Sigma with a purity of 98%. The liquid sample was heated up to 70°C [20] and introduced into the chamber with a nozzle with an orifice of 75 μm . We flowed helium as a carrier gas to increase the electron scattering intensity with a backing pressure of 100 torr. The UV laser pulse energy is 60 μJ for iodobenzene experiment, which is in the range of one photon excitation.

At the interaction region, the gas jet is perpendicular to the plane created by the laser and electron beams. The group velocity mismatch between the electron and laser pulses at the sample is compensated by introducing an angle of 58° between the laser and electron beams and by tilting the laser intensity front with respect to the laser phase front by an angle of 58°. The overall temporal resolution of the UED setup has been characterized to be 214 ± 22 fs FWHM [65]. The electron diffraction patterns are detected by a phosphor screen that is imaged onto an electron-multiplying charge-coupled device. The directly transmitted electron beam is collected by a copper beam stop, which makes a shadow on the detector where the diffraction signal cannot be recorded.

APPENDIX B: DATA PROCESSING PROCEDURES

The procedures for calculating the experimental $\Delta sM(s, t)$ for the photodissociation experiment of CF_3I and iodobenzene are described below. 1st, the

data in the shadow of the beam stop and outliers are removed from each diffraction image for the analysis. 2nd, the 2D diffraction-difference patterns are calculated by taking the difference between the patterns at positive time delays and the reference patterns at negative time delays, given by $\Delta I_M(s, t) = I_{total}(s, t) - I_{total}(s, t < 0)$, where the time zero ($t=0$) is defined as the time at which the dissociation signal becomes visible. 3rd, $\Delta I_M(s, t)$ is azimuthally averaged to calculate the 1D diffraction-difference intensity $\Delta I_M(s, t)$. 4th, the experimental $\Delta sM(s, t)$ at each time delay is calculated using Eqn. (7). 5th, the residual background in the $\Delta sM(s, t)$ is removed. A third-order polynomial is first fit to the $\Delta sM(s, t)$ to approximate the residual background and is then removed from the signal [44]. 6th, the time range of CF₃I experiment spanned from -0.5 ps up to 2 ps, with a time step of 133.3 fs [63]. The $\Delta sM(s, t)$ from 0.2 ps to 2 ps are averaged to obtain $\Delta sM(s)$ shown in figure 14. For iodobenzene signal, the time range spanned from -0.8 ps to around 10 ps. The $\Delta sM(s, t)$ from 1 ps to ~10 ps are averaged to obtain $\Delta sM(s)$ shown in figure 16.

APPENDIX C: SIMULATED X-RAY DIFFRACTION SIGNAL

In ultrafast scattering studies, the molecular dynamics can also be captured using X-ray diffraction. Despite a great achievement in the time resolution, the diffraction data also suffers the loss of low momentum transfer region due to the un-scattered X-ray. Therefore, by only utilizing the available experimental signal and Fourier transform back and forth between reciprocal and real space, our proposed method could, in principle, also be applicable to retrieve the signal in low momentum region in the X-ray data.

Similar to electron scattering theory, the total elastic X-ray scattering constitutes atomic scattering $I_A(s)$, and molecular scattering $I_M(s)$ are given by [48, 49]

$$I_{total}(s) = I_A(s) + I_M(s), \quad (19)$$

$$I_A(s) = \sum_{i=1}^N |F_i(s)|^2, \quad (20)$$

$$I_M(s) = \sum_{i=1}^N \sum_{j=1, j \neq i}^N F_i^*(s) F_j(s) \frac{\sin(sr_{ij})}{sr_{ij}}, \quad (21)$$

where N is the number of atoms that constituent the molecule, s is the momentum transfer with magnitude $s = \frac{4\pi}{\lambda} \sin(\frac{\theta}{2})$, in which λ is the wavelength and θ is the scattered angle of X-ray photon, $F_j(s)$ is the X-ray elastic scattering amplitude of the j th atom, and r_{ij} is the interatomic distance between i th atom and j th atom. Note that the momentum transfer is usually denoted as q in literature of X-ray diffraction, whereas here it is denoted as s to avoid confusion.

We applied the proposed iterative algorithm to the simulated X-ray diffraction signal with the X-ray energy at 15 keV. The useful data in X-ray experiments is usually from around 0.5 \AA^{-1} to 4.5 \AA^{-1} [2, 51, 52]. To demonstrate the capability of the algorithm, the available momentum transfer of the simulated signal is from 1 to 4 \AA^{-1} , and we aim to retrieve the signal between 0 and 1 \AA^{-1} . The procedures of retrieval are the same as the procedures described in section III in main text.

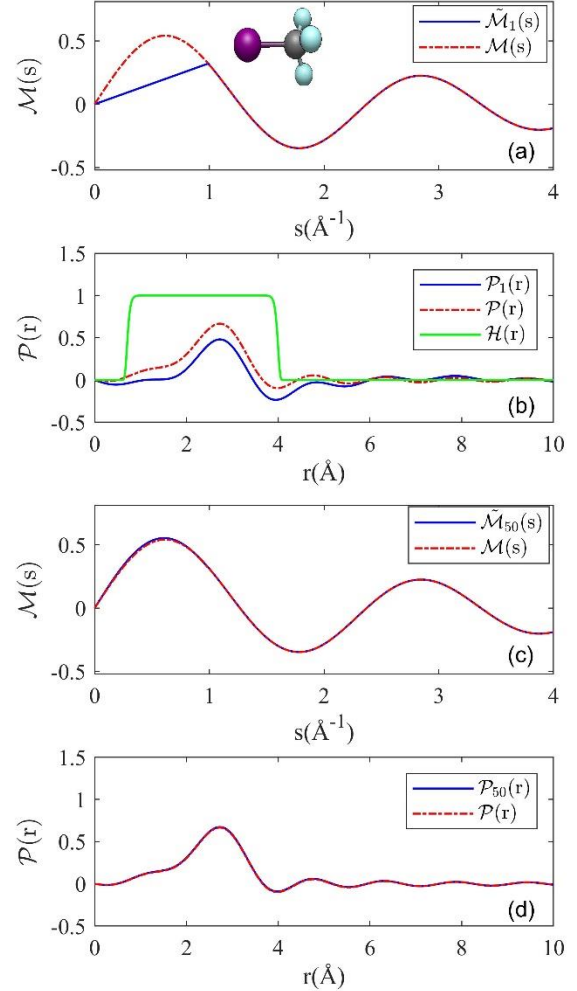


Figure 19. Restoring the simulated X-ray diffraction data of CF₃I in the ground state. (a) $\tilde{\mathcal{M}}_1(s)$ is the signal with the missing region from 0 to 1 \AA^{-1} , which is the blue solid line and is the input for the 1st iteration. The calculated signal without the missing region, $\mathcal{M}(s)$, is the red dashed line, used as a reference for comparison. The inset is the structure of a CF₃I molecule, where the iodine atom is purple, the carbon atom is grey, and the fluorine atoms are green. (b) The Fourier sine transform of $\tilde{\mathcal{M}}_1(s)$ and $\mathcal{M}(s)$ are the blue and red dashed lines, denoted as $\mathcal{P}_1(r)$ and $\mathcal{P}(r)$, respectively. The band-pass filter $\mathcal{H}(r)$ is the green

line. (c) The restored signal after 50 iterations, denoted as $\tilde{\mathcal{M}}_{50}(s)$, is shown by the blue line. The red dashed line is $\mathcal{M}(s)$. (d) The Fourier transform of $\tilde{\mathcal{M}}_{50}(s)$ produces $\mathcal{P}_{50}(r)$, shown with the blue line. The red dashed line is $\mathcal{P}(r)$.

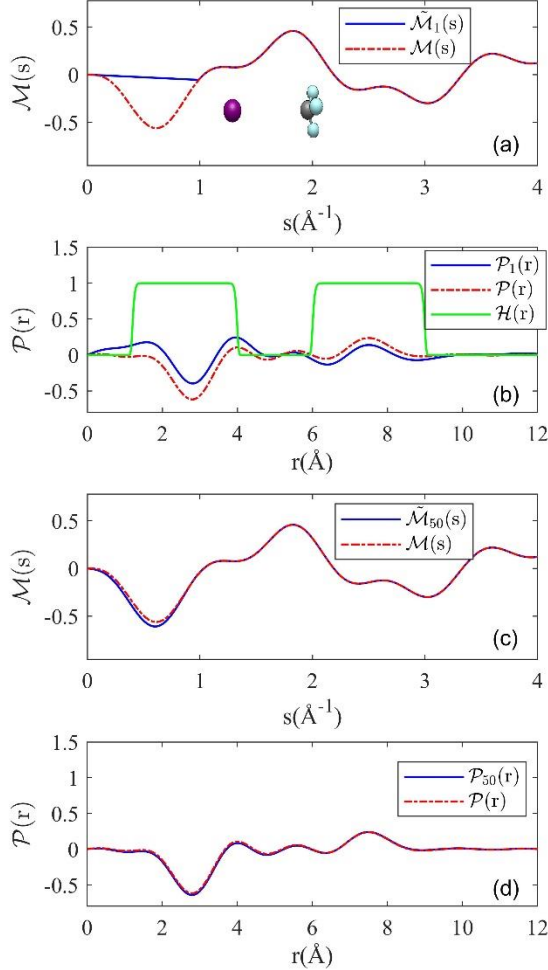


Figure 20. Restoring the simulated X-ray diffraction data of CF_3I , where the CI distance of a CF_3I molecule is elongated by 5\AA . (a) $\tilde{\mathcal{M}}_1(s)$ is the signal with the missing region from 0 to 1\AA^{-1} , which is the blue solid line and is the input for the 1st iteration. The calculated signal without the missing region, $\mathcal{M}(s)$, is the red dashed line, used as a reference for comparison. The inset is the structure of a CF_3I molecule with the CI interatomic distance elongated by 5\AA , where the iodine atom is purple, the carbon atom is grey, and the fluorine atoms are green. (b) The Fourier sine transform of $\tilde{\mathcal{M}}_1(s)$ and $\mathcal{M}(s)$ are the blue and red dashed lines, denoted as $\mathcal{P}_1(r)$ and $\mathcal{P}(r)$, respectively. The band-pass filter $\mathcal{H}(r)$ is the green line. (c) The restored signal after 50 iterations, denoted as $\tilde{\mathcal{M}}_{50}(s)$, is shown by the blue line. The red dashed line is $\mathcal{M}(s)$.

(d) The Fourier transform of $\tilde{\mathcal{M}}_{50}(s)$ produces $\mathcal{P}_{50}(r)$, shown with the blue line. The red dashed line is $\mathcal{P}(r)$.

Figure 19 shows the retrieval result of CF_3I in the ground state, and figure 20 shows the retrieval of CF_3I with the CI distance increased by 5\AA . Although the X-ray scattering signal is limited by a small region of momentum transfer due to low scattering cross section, making the interatomic distances unresolvable as shown in figure 19(b) and 20(b), the algorithm is still able to retrieve the correct signal in low s region. A very good agreement between retrieved signal and reference is achieved after 50 iterations and is shown in figure 19(c)-(d) and 20(c)-(d). This successful retrieval highlights the applicability of the proposed iterative algorithm to the general diffraction data.

1. Centurion, M., T.J.A. Wolf, and J. Yang, *Ultrafast Imaging of Molecules with Electron Diffraction*. Annu Rev Phys Chem, 2022. **73**: p. 21-42.
2. Minitti, M.P., et al., *Imaging Molecular Motion: Femtosecond X-Ray Scattering of an Electrocyclic Chemical Reaction*. Phys Rev Lett, 2015. **114**(25): p. 255501.
3. Zandi, O., et al., *High current table-top setup for femtosecond gas electron diffraction*. Structural Dynamics, 2017. **4**(4): p. 044022.
4. Xiong, Y., K.J. Wilkin, and M. Centurion, *High-resolution movies of molecular rotational dynamics captured with ultrafast electron diffraction*. Physical Review Research, 2020. **2**(4).
5. Ihee, H., et al., *Ultrafast Electron Diffraction and Structural Dynamics: Transient Intermediates in the Elimination Reaction of C2F4I2*. The Journal of Physical Chemistry A, 2002. **106**(16): p. 4087-4103.
6. Park, S.T., et al., *Ultrafast electron diffraction reveals dark structures of the biological chromophore indole*. Angew Chem Int Ed Engl, 2008. **47**(49): p. 9496-9.
7. Wang, Y., et al., *Ultrafast electron diffraction instrument for gas and condensed matter samples*. Rev Sci Instrum, 2023. **94**(5).
8. Yang, J., et al., *Femtosecond gas phase electron diffraction with MeV electrons*. Faraday Discuss, 2016. **194**: p. 563-581.
9. Shen, X., et al., *Femtosecond gas-phase mega-electron-volt ultrafast electron diffraction*. Struct Dyn, 2019. **6**(5): p. 054305.
10. Weathersby, S.P., et al., *Mega-electron-volt ultrafast electron diffraction at SLAC*.

11. Ma, Z., et al., *Ultrafast isolated molecule imaging without crystallization*. Proc Natl Acad Sci U S A, 2022. **119**(15): p. e2122793119.
12. Xiong, Y. and M. Centurion, *Fast calculation of diffraction patterns from an ensemble of aligned molecules*. Physical Review A, 2025.
13. Srinivasan, R., et al., *Ultrafast Electron Diffraction (UED). A New Development for the 4D Determination of Transient Molecular Structures*. Cheminform, 2003. **34**(40): p. págs. 1761-1838.
14. Ihee, H., et al., *Direct imaging of transient molecular structures with ultrafast diffraction*. Science, 2001. **291**(5503): p. 458-62.
15. Srinivasan, R., et al., *Dark structures in molecular radiationless transitions determined by ultrafast diffraction*. Science, 2005. **307**(5709): p. 558-63.
16. Yang, J., et al., *Imaging of alignment and structural changes of carbon disulfide molecules using ultrafast electron diffraction*. Nature communications, 2015. **6**.
17. Wilkin, K.J., et al., *Ultrafast electron diffraction from transiently aligned asymmetric top molecules: Rotational dynamics and structure retrieval*. Structural Dynamics, 2022. **9**(5): p. 054303.
18. Hensley, C.J., J. Yang, and M. Centurion, *Imaging of isolated molecules with ultrafast electron pulses*. Physical review letters, 2012. **109**(13): p. 7035-7040.
19. Yang, J., et al., *Diffraction imaging of a rotational wavepacket in nitrogen molecules with femtosecond megaelectronvolt electron pulses*. Nature communications, 2016. **7**.
20. Xiong, Y., et al., *Retrieval of the molecular orientation distribution from atom-pair angular distributions*. Physical Review A, 2022. **106**(3).
21. Reckenthaeler, P., et al., *Time-resolved electron diffraction from selectively aligned molecules*. Physical review letters, 2009. **102**(21).
22. Yang, J., et al., *Imaging CF₃I conical intersection and photodissociation dynamics with ultrafast electron diffraction*. Science, 2018. **361**(6397): p. 64-67.
23. Yang, J., et al., *Diffraction Imaging of Coherent Nuclear Motion in Isolated Molecules*. Phys Rev Lett, 2016. **117**(15): p. 153002.
24. Reckenthaeler, P., et al., *Time-resolved electron diffraction from selectively aligned molecules*. Phys Rev Lett, 2009. **102**(21): p. 213001.
25. Hensley, C.J., J. Yang, and M. Centurion, *Imaging of isolated molecules with ultrafast electron pulses*. Physical review letters, 2012. **109**(13): p. 133202.
26. Yang, J., et al., *Diffraction imaging of a rotational wavepacket in nitrogen molecules with femtosecond megaelectronvolt electron pulses*. Nat Commun, 2016. **7**(1): p. 11232.
27. Wang, T., et al., *Imaging the photochemical dynamics of cyclobutanone with MeV ultrafast electron diffraction*. The Journal of Chemical Physics, 2025. **162**(18).
28. Xu, S., et al., *Ultrafast Electron Diffraction: Structural Dynamics of the Elimination Reaction of Acetylacetone*. The Journal of Physical Chemistry A, 2004. **108**(32): p. 6650-6655.
29. Ruan, C.Y., et al., *Ultrafast diffraction and structural dynamics: the nature of complex molecules far from equilibrium*. Proc Natl Acad Sci U S A, 2001. **98**(13): p. 7117-22.
30. Muvva, S.B., et al., *Ultrafast structural dynamics of UV photoexcited cis, cis-1, 3-cyclooctadiene observed with time-resolved electron diffraction*. Physical Chemistry Chemical Physics, 2025. **27**(1): p. 471-480.
31. Figueira Nunes, J.P., et al., *Monitoring the Evolution of Relative Product Populations at Early Times during a Photochemical Reaction*. Journal of the American Chemical Society, 2024. **146**(6): p. 4134-4143.
32. Fienup, J.R., *Phase retrieval algorithms: a comparison*. Appl Opt, 1982. **21**(15): p. 2758-69.
33. Saxton, W.O., L. Marton, and C. Marton, *Computer Techniques for Image Processing in Electron Microscopy*. 2013: Academic Press.
34. Gerchberg, R.W., *A practical algorithm for the determination of phase from image and diffraction plane pictures*. Optik, 1972. **35**: p. 237-246.
35. Elser, V., *Phase retrieval by iterated projections*. Journal of the Optical Society of America A, 2003. **20**(1): p. 40-55.
36. Bauschke, H.H., P.L. Combettes, and D.R. Luke, *Phase retrieval, error reduction algorithm, and Fienup variants: a view from convex optimization*. Journal of the Optical Society of America A, 2002. **19**(7): p. 1334-1345.

37. Marchesini, S., *Invited article: a [corrected] unified evaluation of iterative projection algorithms for phase retrieval*. Rev Sci Instrum, 2007. **78**(1): p. 011301.
38. Fienup, J.R., *Reconstruction of an object from the modulus of its Fourier transform*. Optics Letters, 1978. **3**(1): p. 27-29.
39. Marchesini, S., et al., *X-ray image reconstruction from a diffraction pattern alone*. Physical Review B, 2003. **68**(14): p. 140101.
40. Brockway, L.O., *Electron Diffraction by Gas Molecules*. Reviews of Modern Physics, 1936. **8**(3): p. 231-266.
41. Karle, J., *Electron Diffraction*, in *Determination of Organic Structures by Physical Methods*, F.C. Nachod and J.J. Zuckerman, Editors. 1973, Academic Press. p. 1-74.
42. Williamson, J.C. and A.H. Zewail, *Ultrafast Electron Diffraction. 4. Molecular Structures and Coherent Dynamics*. The Journal of Physical Chemistry, 1994. **98**(11): p. 2766-2781.
43. Hargittai, I. and M. Hargittai, *Stereochemical Applications of Gas-Phase Electron Diffraction*. 1988: Wiley.
44. Xiong, Y., et al., *Strong-field induced fragmentation and isomerization of toluene probed by ultrafast femtosecond electron diffraction and mass spectrometry*. Faraday Discuss, 2021.
45. Yang, J., et al., *Simultaneous observation of nuclear and electronic dynamics by ultrafast electron diffraction*. Science, 2020. **368**(6493): p. 885-889.
46. Mott, N.F., *The scattering of electrons by atoms*. Proceedings of the Royal Society of London. Series A, Containing Papers of a Mathematical and Physical Character, 1930. **127**(806): p. 658-665.
47. Bethe, H., *Zur Theorie des Durchgangs schneller Korpuskularstrahlen durch Materie*. Annalen der Physik, 1930. **397**(3): p. 325-400.
48. Debye, P., *Scattering from non-crystalline substances*. Ann. Physik, 1915. **46**: p. 809-823.
49. Ehrenfest, P., *On interference phenomena to be expected when Roentgen rays pass through a di-atomic gas*. Koninklijke Nederlandse Akademie van Wetenschappen Proceedings Series B Physical Sciences, 1915. **17**: p. 1184-1190.
50. Prince, E., *International Tables for Crystallography Volume C: Mathematical, physical and chemical tables*. 2004. C.
51. Yong, H., et al., *Ultrafast X-ray scattering offers a structural view of excited-state charge transfer*. Proceedings of the National Academy of Sciences, 2021. **118**(19): p. e2021714118.
52. Budarz, J.M., et al., *Observation of femtosecond molecular dynamics via pump-probe gas phase x-ray scattering*. Journal of Physics B: Atomic, Molecular and Optical Physics, 2016. **49**(3): p. 034001.
53. 16843, P.C.S.f.C. *Trifluoroiodomethane*. 2025; Available from: <https://pubchem.ncbi.nlm.nih.gov/compound/Trifluoroiodomethane>.
54. 11575, P.C.S.f.C. *Iodobenzene*. 2025; Available from: <https://pubchem.ncbi.nlm.nih.gov/compound/Iodobenzene>.
55. Dzvonik, M., S. Yang, and R. Bersohn, *Photodissociation of molecular beams of aryl halides*. The Journal of Chemical Physics, 1974. **61**(11): p. 4408-4421.
56. Durie, R.A., T. Iredale, and J.M.S. Jarvie, *Absorption spectra of substances containing the carbon-iodine bond. Part I*. Journal of the Chemical Society (Resumed), 1950: p. 1181-1184.
57. Van Veen, G.N.A., et al., *Photofragmentation of CF3I in the A band*. Chemical Physics, 1985. **93**(2): p. 277-291.
58. Cheng, P.Y., D. Zhong, and A.H. Zewail, *Kinetic-energy, femtosecond resolved reaction dynamics. Modes of dissociation (in iodobenzene) from time-velocity correlations*. Chemical Physics Letters, 1995. **237**(5): p. 399-405.
59. Sage, A.G., et al., *nsigma* and pisigma* excited states in aryl halide photochemistry: a comprehensive study of the UV photodissociation dynamics of iodobenzene*. Phys Chem Chem Phys, 2011. **13**(18): p. 8075-93.
60. Zhang, X.P., W.B. Lee, and K.C. Lin, *Nonadiabatic transition in the A-band photodissociation of ethyl iodide from 294 to 308 nm by using velocity imaging detection*. J Phys Chem A, 2009. **113**(1): p. 35-9.
61. Mulliken, R.S., *Intensities in Molecular Electronic Spectra X. Calculations on Mixed-Halogen, Hydrogen Halide, Alkyl Halide, and Hydroxyl Spectra*. The Journal of Chemical Physics, 1940. **8**(5): p. 382-395.

- 62. Yin, S., et al., *Femtosecond pump-probe mass spectra on the dissociative photoionization of CF₃I*. Chemical Physics Letters, 2003. **372**(5): p. 904-910.
- 63. Xiong, Y., *Diffractional Imaging of Laser Induced Molecular Reactions with Kilo-electron-Volt Ultrafast Electron Diffraction*. 2023, The University of Nebraska - Lincoln: United States -- Nebraska. p. 170-173.
- 64. Le, C., Y. Xiong, and M. Centurion, *Direct structural retrieval from gas-phase ultrafast diffraction data using a genetic algorithm*. Physical Review A, 2025. **112**(5).
- 65. Wang, Y., et al., *Ultrafast dynamics of ferroelectric polarization of NbOI₂ captured with femtosecond electron diffraction*. Nature Communications, 2025. **16**(1): p. 8132.